Theoretical analysis of backscattering in hollow-core antiresonant fibers

Eric Numkam Fokoua,[1, a)] Vincent Michaud-Belleau,[2] Jérôme Genest,[2] Radan Slavík,[1] and Francesco Poletti[1]
[1)]*Optoelectronics Research Centre, University of Southampton, Southampton, SO17 1BJ, UK*
[2)]*Centre d'optique, photonique et laser, Université Laval, Québec, Québec, G1V 0A6, Canada*

(Dated: 24 August 2021)

We present a theoretical analysis into the fundamental physical mechanisms contributing to backscattering in hollow-core antiresonant fibers. We consider Rayleigh scattering originating from the hollow regions of the fiber which may be filled with gases, Rayleigh scattering from within the glass membranes as well as the contribution from scattering at the glass surfaces. We derive expressions for the backscattering coefficient into any specified guided mode for an arbitrary excitation. These lead to general scaling relations with the core size and wavelength which are found to be the key parameters for backscattering, regardless of the exact antiresonant geometry. For a nested antiresonant hollow-core fiber with a core diameter of 35 μm, the only antiresonant fiber geometry for which experimental data is available in the literature, we find that the surface-scattering limited backscattering coefficient of the fundamental mode into itself is nearly 40 dB below that of a single mode fiber, in good agreement with recently published measurements.

I. INTRODUCTION

Over the past few years, hollow-core optical fiber research has gained renewed interest, driven primarily by the sustained and rapid improvement in their performance. The lowest loss which has been obtained in the nested antiresonant nodeless geometry (NANF) now stands at 0.28 dB/km at 1550 nm, a factor of two above the Rayleigh scattering limit of conventional single mode fibers (SMF)[1]. Furthermore, these fibers have now achieved lower loss than conventional silica fibers at wavelengths in the visible and mid infrared, and are predicted to outperform standard fibers at any technologically relevant wavelengths[2–4]. Beyond lower attenuation, they offer significant advantages over their conventional counterparts, including nearly three orders of magnitude lower optical nonlinearity and near vacuum latency. For hollow-core fibers based on antiresonance guidance, there are further advantages like low chromatic dispersion and, as recently shown, high polarization purity and very low levels of backscattering[5,6]. Such low levels of backscattering, measured to be more than 40 dB lower than in SMFs, are especially beneficial for applications relying on bidirectional propagation, for example in fiber optic gyroscopes[7], remote fiber sensors interrogated in reflection[8], or bidirectional fiber links used in time and frequency transfer[9].

The rapid pace of development of hollow-core antiresonant fibers has not permitted a thorough understanding of some of their most striking properties[1,10,11]. Backscattering is one such example where practical demonstration of ultralow backscattering levels has preceded a detailed understanding of the physical mechanisms that contribute to it[6]. However, such an understanding is necessary for at least two reasons. The first is to establish general sensitivity requirements for reflectometry-based tools that may be routinely used for distributed fault-finding in manufactured fibers and cables. The second is to guide the design of fibers with ultralow backscattering to serve applications such as optical gyroscopes or quantum key distribution where it can severely limit performance.

In this paper, we present a theoretical analysis of the optical backscattering process in hollow-core antiresonant fibers. We derive expressions for each contribution and establish general scaling relations with wavelength and core size. We show that the scattering from surface roughness imposes a fundamental limit on backscattering. However, when filled with a gas at a sufficient pressure level (e.g., air at atmospheric pressure), Rayleigh scattering from within the hollow regions can become the dominant contribution to the backscattering signal.

II. THEORETICAL ANALYSIS

As in any waveguide, light scattering in antiresonant fibers originates from random small-scale inhomogeneities in the local permittivity distribution. Such inhomogeneities consist of density fluctuations within the glass microstructure and in the gas-filled hollow regions of the fiber (naturally, this component vanishes if the hollow regions are evacuated), and also, of the roughness and inhomogeneities at the glass surfaces. Such roughness is known to be fundamentally limited by frozen-in thermally-excited surface capillary waves and contributes to loss and backscattering by the fiber[12].

Coupled-mode analysis offers a formalism for analyzing such perturbation effects[13,14]. Here however, we make use of the volume current method which yields identical results but permits a more intuitive analysis[15–18]. We first compute the current density induced by the presence of volumetric and surface inhomogeneities, then find the mode amplitudes excited by such a current density from which we obtain the backscattering coefficients.

In the absence of any perturbation, the longitudinally invariant (ideal) antiresonant fiber supports a set of discrete guided modes (although leaky in this case) complemented by a continuum of cladding and radiation modes. We will express such

[a)]Electronic mail: Eric.Numkam-Fokoua@soton.ac.uk

solutions in the form:

$$|\psi_k^{(p)}\rangle = \begin{pmatrix} \mathbf{E}_t^{(p)} \\ \mathbf{H}_t^{(p)} \end{pmatrix}_k e^{-j\beta_k^{(p)} z} \quad (1)$$

where k serves to label the modes, the subscript t indicates transverse field components, the superscript $p = (+)$ or $(-)$ indicates the direction of propagation and $\beta_k^{(p)}$ the propagation constant. Because the ideal fiber has reflection symmetry about any plane orthogonal to its axis, backward propagating modes can be expressed as: $\beta_k^{(-p)} = -\beta_k^{(p)}$, $\mathbf{E}_t^{(-p)} = \mathbf{E}_t^{(p)}$, $\mathbf{H}_t^{(-p)} = -\mathbf{H}_t^{(p)}$ (see[19]). Consequently, the longitudinal components satisfy: $\mathbf{E}_z^{(-p)} = -\mathbf{E}_z^{(p)}$, $\mathbf{H}_z^{(-p)} = \mathbf{H}_z^{(p)}$. These modes form a complete set and obey the orthonormality relation[20]:

$$\iint_{A_\infty} \vec{z} \cdot \left(\mathbf{E}_{tk}^{(p)} \times \mathbf{H}_{tl}^{(q)*} + \mathbf{E}_{tl}^{(q)*} \times \mathbf{H}_{tk}^{(p)} \right) dA = \zeta_p \delta_{kl} \delta_{pq} \quad (2)$$

Here, $\zeta_p = 1$ if $p = +$ or -1 otherwise and δ_{mn} is the Kronecker delta, being 1 if $m = n$ and 0 otherwise.

We now consider that the mode $|\psi_k^{(p)}\rangle$ carrying unit power is incident on a section of fiber of length L in the p direction. The presence of small perturbations can be regarded as giving rise to an equivalent induced current density $\mathbf{J}_k^{(p)}$. The perturbed waveguide is thus approximated as the ideal unperturbed waveguide and a source term which is the equivalent current density. With the mode normalization above, such an equivalent current density in turn results in the excitation of mode $|\psi_l^{(q)}\rangle$ with unitless amplitude[21,22]:

$$a_{kl}^{(pq)} = \int_0^L \iint_{A_\infty} \mathbf{E}_l^{(q)*} \cdot \mathbf{J}_k^{(p)} dA dz \quad (3)$$

The scattering coefficient per unit length from mode $|\psi_k^{(p)}\rangle$ into mode $|\psi_l^{(q)}\rangle$ is therefore:

$$B_{kl}^{(pq)} = \frac{1}{L} \left\langle a_{kl}^{(pq)*} a_{kl}^{(pq)} \right\rangle \quad (4)$$

where $\langle \ldots \rangle$ represents an ensemble average over statistically equivalent fiber sections. When L is sufficiently short that the relevant modes do not suffer appreciable loss over the section, the backscattering coefficient for mode $|\psi_k^{(p)}\rangle$ may thus be rigorously defined as:

$$B_k = \sum_{l,q \neq p} B_{kl}^{(pq)} = \frac{1}{L} \sum_{l,q \neq p} \left\langle a_{kl}^{(pq)*} a_{kl}^{(pq)} \right\rangle \quad (5)$$

Here, the summation extends over all the modes propagating in the direction opposite to that of the incident mode. In practice however, we are interested in backward propagating guided modes in the core and more often still, the backward propagating fundamental mode alone.

We distinguish two types of inhomogeneities that may give rise to an induced current density: density fluctuations leading to volumetric Rayleigh scattering in the gas-filled hollow regions and within the glass regions, and roughness at the air-glass interfaces. We analyze them below in greater detail.

A. Volumetric Rayleigh scattering contribution to backscattering

Small-scale density fluctuations within the glass or the gas in the hollow regions of the fiber are effectively represented by a small perturbation of the relative dielectric permittivity $\Delta\varepsilon_r(x,y,z)$. Because such a perturbation is typically very small in magnitude, the shape of the perturbed region plays a negligible role and the equivalent current density when mode $|\psi_k^{(p)}\rangle$ is incident on the fiber section is simply given by[14,23]:

$$\mathbf{J}_k^{(p)} = -j\omega\varepsilon_0 \Delta\varepsilon_r(x,y,z) \mathbf{E}_k^{(p)} \quad (6)$$

By inserting this expression into Eq. 3 and 4, we obtain the volumetric scattering into mode $|\psi_l^{(q)}\rangle$ as:

$$B_{kl}^{(pq)} = \frac{1}{L} \omega^2 \varepsilon_0^2 \int_V \int_V \left\langle \Delta\varepsilon_r(x',y',z') \Delta\varepsilon_r(x,y,z) \right\rangle \left(\mathbf{E}_l^{(q)}(x',y') \cdot \mathbf{E}_k^{(p)*}(x',y') \right) \left(\mathbf{E}_l^{(q)*}(x,y) \cdot \mathbf{E}_k^{(p)}(x,y) \right) e^{-j\left(\beta_k^{(p)} - \beta_l^{(q)}\right)(z-z')} dx'dy'dz'dxdydz \quad (7)$$

For a Rayleigh scattering process, the permittivity perturbations are very rapid compared to the wavelength, and in that case, the form of their autocorrelation function can be taken as a delta function[13,24] :

$$\left\langle \Delta\varepsilon_r(x',y',z') \Delta\varepsilon_r(x,y,z) \right\rangle = l_c^3 \left\langle \Delta\varepsilon_r^2 \right\rangle \times \delta(x-x')\delta(y-y')\delta(z-z') \quad (8)$$

Where l_c is the correlation length of the perturbation and $\langle \Delta\varepsilon_r^2 \rangle$ the variance of the relative permittivity fluctuation. With this definition, the relevant Rayleigh scattering coefficient is expressed as $\alpha_R = k^4 l_c^3 \langle \Delta\varepsilon_r^2 \rangle / 6\pi$ (see[21]). If the perturbed material occupies a region A in the cross section, then by substituting Eq. 8 into Eq. 7, the backscattering coefficient reduces to:

$$B_{kl}^{(pq)} = \frac{6\pi}{k^4} \omega^2 \varepsilon_0^2 \alpha_R \iint_A \left| \mathbf{E}_l^{(q)*}(x,y) \cdot \mathbf{E}_k^{(p)}(x,y) \right|^2 dxdy \quad (9)$$

In antiresonant fibers, A may be the area covered by the gas-filled hollow regions or that covered by the glass, allowing to calculate volumetric contributions to backscattering from either gas or glass.

Eq. 9 yields identical results to those obtained in[21] when considering a single mode fiber, or those obtained for solid core few-moded fibers using the diffraction method[25], but it is more general. To confirm this, we consider a standard single mode fiber in which the linearly polarized and nearly Gaussian forward propagating mode field ($\mathbf{E}_\mathbf{0}^+ = \vec{x} E_0 e^{-r^2/W_0^2}$, W_0 is the mode spot radius) carries unit power (that is, $E_0^2 = 4/(\pi W_0^2 n)\sqrt{\mu_0/\varepsilon_0}$). Since the backward propagating mode field is identical under this simple approximation, after renormalizing the mode field amplitude according to Eq. 2,

Eq. 9 yields:

$$B = \frac{6\pi}{k^4}\omega^2\varepsilon_0^2\alpha_R\int_0^{2\pi}\int_0^{\infty}\frac{\mu_0/\varepsilon_0}{\pi^2 n^2 W_0^4}e^{-4r^2/W_0^2}rdrd\theta = \alpha_R\frac{3}{2n^2W_0^2(\omega/c)^2} \quad (10)$$

which is the well-known result for SMFs under this Gaussian approximation[21,26,27].

B. Surface contributions to backscattering

It is now well accepted that in hollow-core fibers, the air-glass interfaces possess intrinsic nanoscale roughness from frozen-in thermally excited surface capillary waves[12,28]. Light scattered by these rough interfaces gives rise to loss and backscattering.

Since the refractive index contrast between a potential filling gas (or vacuum) and glass, of the order of $\varepsilon_{r1}:\varepsilon_{r2}\sim 1{:}2$, is high enough to cause a local discontinuity of the electric field distribution near the glass surfaces, an appropriate expression for the induced current density from surface roughness must employ only field quantities that are continuous across the interfaces[23,29]. These are the components of the electric field parallel to the interface $\mathbf{E}_{\|}$ and the component of the electric displacement normal to the interfaces $\mathbf{D}_{\perp}$. Assuming that the geometric perturbations caused by roughness on the air-glass interfaces are described by a small deviation $h(s,z)$ (s is a curvilinear coordinate along the interface in the cross-section) that does not change the local surface normal nor the refractive index, the induced current density by the incident mode $|\psi_k^{(p)}\rangle$ is expressed as[23,29]:

$$\mathbf{J}_k^{(p)} = -i\omega\varepsilon_0\left(\Delta\varepsilon_r\mathbf{E}_{\|k}^{(p)}(s) - \Delta\frac{1}{\varepsilon_r}\mathbf{D}_{\perp k}^{(p)}(s)\right)h(s,z) \quad (11)$$

Here, $\Delta\varepsilon_r = n_{glass}^2 - 1$ and $\Delta 1/\varepsilon_r = 1/n_{glass}^2 - 1$. If we now assume that the roughness on each of the air glass interfaces is statistically independent, then by inserting Eq. 11 into Eqs. 3 and 4, we obtain the scattering into mode $|\psi_l^{(q)}\rangle$ as:

$$B_{kl}^{(pq)} = \frac{1}{L}\omega^2\varepsilon_0^2\sum_j\int_0^L\int_0^L\oint_{S_j}\oint_{S_j}\langle h(s',z')h(s,z)\rangle\left(\Delta\varepsilon_r\mathbf{E}_{\|l}^{(q)}(s')\cdot\mathbf{E}_{\|k}^{(p)*}(s') - \Delta\tfrac{1}{\varepsilon_r}\mathbf{D}_{\perp l}^{(q)}(s')\mathbf{D}_{\perp k}^{(p)*}(s')\right)$$
$$\left(\Delta\varepsilon_r\mathbf{E}_{\|l}^{(q)*}(s)\cdot\mathbf{E}_{\|k}^{(p)}(s) - \Delta\tfrac{1}{\varepsilon_r}\mathbf{D}_{\perp l}^{(q)*}(s)\mathbf{D}_{\perp k}^{(p)}(s)\right)e^{-j\left(\beta_k^{(p)}-\beta_l^{(q)}\right)(z-z')}ds'dsdz'dz \quad (12)$$

Eq. 12 can be further simplified only if the roughness autocorrelation $\langle h(s',z')h(s,z)\rangle$ is separable, i.e., can be written as a product of functions of $s-s'$ and $z-z'$. This not the case for frozen-in surface capillary waves, making the evaluation of the integral in Eq. 12 complicated[28,30]. We argue however that the most important features of the roughness, especially those dictating the angular distribution of the scattered light are those along the fiber axis. With this assumption and the choice of the section length L so that it is longer than the wavelength and any relevant correlation length of the roughness, yet short enough that the modes do not suffer very high losses, Eq. 12 simplifies to:

$$B_{kl}^{(pq)} = \omega^2\varepsilon_0^2\tilde{\Psi}\left(\beta_k^{(p)}-\beta_l^{(q)}\right)\times \sum_j\left|\oint_{S_j}\left(\Delta\varepsilon_r\mathbf{E}_{\|l}^{(q)*}(s)\cdot\mathbf{E}_{\|k}^{(p)}(s) - \Delta\frac{1}{\varepsilon_r}\mathbf{D}_{\perp l}^{(q)*}(s)\mathbf{D}_{\perp k}^{(p)}(s)\right)ds\right|^2 \quad (13)$$

Here, $\tilde{\Psi}(\Delta\beta)$ is the power spectral density of the roughness in the z direction, which we have assumed is the same for all the air-glass interfaces for simplicity.

Throughout the remainder of the paper, we will limit our analysis to backscattering caused by frozen-in surface capillary waves since its thermodynamic origin makes it the only true fundamental limit to surface scattering which cannot be removed through technological improvements in the fabrication process. For this roughness, the power spectrum is given by[28,30]:

$$\tilde{\Psi}(\Delta\beta) = \frac{k_B T_g}{4\pi\gamma\sqrt{\kappa_c^2+\Delta\beta^2}} \quad (14)$$

where k_B is Boltzmann's constant, T_g the glass transition temperature, γ the surface tension, and $\kappa_c = 2\pi/\Lambda_c$ a low frequency cut-off for the roughness spectrum introduced to avoid divergence at long spatial wavelengths and Λ_c is the corresponding spatial wavelength.

C. Scaling relations

It is of interest for many applications to establish how the backscattering coefficient of the fundamental mode into itself (backwards propagating fundamental mode) scales with key fiber design parameters and the operating wavelength.

For the contribution from volumetric scattering in the hollow regions, a scaling relation can be easily obtained from Eq. 9. Away from the resonances where guidance fails ($\lambda_m = 2t\sqrt{n^2-1}/m$, with t being the membrane thickness, n the glass refractive index and m an integer, see peaks in Figs.4 and 5), the integral is proportional to $1/W_0^2$ where W_0 is the mode field radius. Since W_0 is nearly independent of wavelength in antiresonant fibers, it follows that the integral is proportional

to $1/R^2$ (R is the core radius). The multiplying factor scales as ω^2, and it follows therefore that:

$$B_{11}^{gas} \propto \frac{1}{\lambda^2 R^2} \tag{15}$$

The wavelength dependence of the other two contributions is greatly impacted by the guidance mechanism itself. In the vicinity of resonances, the field strength within the glass and near the interfaces changes rapidly with wavelength. However, away from the resonances, simple scaling relations can be obtained. To do so, we note that in the hollow-core fiber, the unnormalized vanishingly small field strength near the air-glass interfaces is proportional to λ/R[20,31]. This implies that to first order, with the normalization of Eq. 2 (i.e, dividing the field by a quantity proportional to $\sqrt{\text{mode area}} \sim R$), the normalized field strength near the interface is proportional to λ/R^2. For the volumetric contribution from glass, the integral in Eq. 9 is carried over an area roughly proportional to the core perimeter and thus proportional to R. It follows therefore from Eq. 9 that away from the resonances, the volumetric contribution from glass satisfies:

$$B_{11}^{glass} \propto \lambda^{-2} \cdot \frac{\lambda^4}{R^8} R \propto \frac{\lambda^2}{R^7} \tag{16}$$

With the power spectrum of Eq. 14 being proportional to $1/\Delta\beta$ and thus to λ, the same argument above leads to the surface contribution to backscattering scaling as:

$$B_{11}^{surf} \propto \lambda^{-2} \cdot \lambda \cdot \left(\frac{\lambda^2}{R^4} \cdot R\right)^2 \rightarrow \frac{\lambda^3}{R^6} \tag{17}$$

III. MODELING EXAMPLES

As a baseline for comparison with hollow-core fibers, we plot in Fig. 1 the modal backscattering coefficients (B_{kl}^{pq}) calculated using Eq. 9 for the first two mode groups of a step index fiber (core diameter: 8.2 µm, NA: 0.14, similar to Corning's SMF28e[32] but simulated both in the single and multimode regimes) as a function of normalized frequency V. The incident power is assumed to be in one of the degenerate fundamental modes labeled 1 and the figure shows the backscattering coefficient of this mode into itself and the other modes labeled 2 to 6, corresponding to the other HE_{11}, and the degenerate TM_{01}, HE_{21} and TE_{01} modes that make up LP_{11} mode group. We drop the superscript $(+-)$ as it is implicitly understood these are backscattering coefficients. Using pure silica's Rayleigh scattering coefficient of 0.8 dB·µm^4/km (see[33]), Eq. 9 predicts a backscattering coefficient of −72.3 dB/m at 1550 nm ($V = 2.32$), in good agreement with typical measured values[32]. Interestingly, in the multimode regime ($V \geq 2.4$), the sum of the backscattering into the higher order mode group is higher than that into the incident fundamental mode, highlighting the importance of considering their contributions in measurements or applications where they can be detected or impact performance.

Using Eq. 9, we repeated these calculations for the volumetric contributions to backscattering from the hollow and glass regions in two different antiresonant fibers, a 7-tube tubular fiber and a NANF with 6 sets of nested tubes[34].

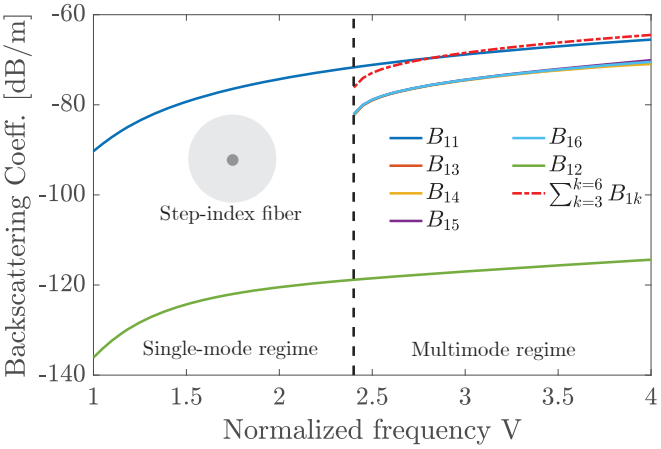

FIG. 1. Backscattering coefficient for the first two mode groups of a step-index solid-glass-core fiber when one of the fundamental modes is incident. The vertical dashed line shows the cut-off frequency $V = 2.405$.

For both fibers, we choose a core diameter of 35 µm and a tube membrane thickness of 400 nm. We solve for the modes of the two fibers using a fully-vectorial commercial finite element solver (COMSOL Multiphysics). Fig. 2 shows the calculated mode field distributions for the fundamental HE_{11} of the two fibers at 1550 nm. We subsequently use the software's postprocessing tools to compute the integral of Eq. 9. The calculated backscattering coefficients are shown in Fig. 3. We assume here that the hollow regions of the fiber are filled with air at room temperature and atmospheric pres-

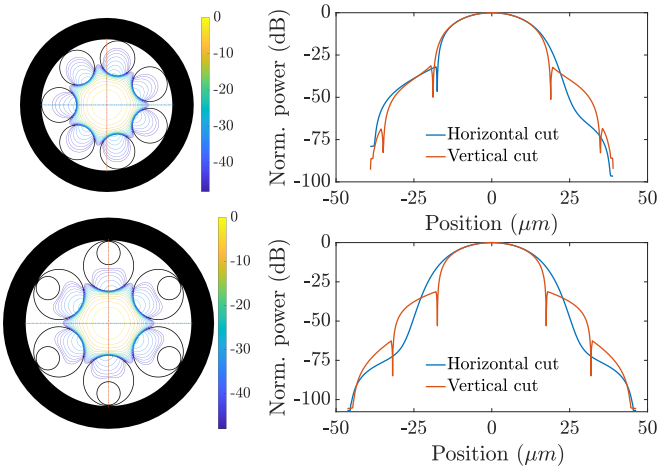

FIG. 2. Calculated mode field distributions in the two antiresonant fibers under study at 1550 nm. The fibers have identical core diameters and membrane thickness, resulting in the NANF being larger than the tubular fiber. The left hand-side shows contour plots of the normalized time-averaged Poynting vector for one of the fundamental modes (we limit the range to [-50, 0] dB) and the right hand side show corresponding cuts along horizontal and vertical lines in both fibers.

sure, thus effectively having a Rayleigh scattering coefficient of 4.7×10^{-3} dB·μm^4/km (see[35]). This choice is arbitrary and for illustrative purposes only as the effective Rayleigh scattering from these regions would depend on the filling gas and its pressure. Just as in the solid-core fiber, we found that the scattering from the hollow regions to the orthogonal polarization of the fundamental mode is nearly four orders of magnitude lower than into itself, and so Fig. 3 does not show them explicitly. For both fibers, the contribution from volumetric Rayleigh scattering in the air-filled hollow regions at 1550 nm is −100 dB/m, some 27 dB below that of the single mode fiber. This is attributed to the lower Rayleigh scattering coefficient of air and the larger mode field diameter of the fundamental mode of the hollow-core fibers (as is evident from Eq. 10). Note that the results are nearly identical for both modeled fibers despite the differences in their structures and symmetry. This is because the mode field distribution is predominantly dictated by the core size, membrane thickness and wavelength. As a result, many of the mode-field dependent properties, including the backscattering would be identical for antiresonant fibers with same core size and membrane thickness, with the exact design of the antiresonant cladding having little impact.

Fig. 4 shows the contribution from Rayleigh scattering in the glass regions for both fibers. At −156 dB/m, this contribution is more than 80 dB below the backscatter level of the SMF. This is due primarily to the very small overlap between the optical field and the glass membranes (for the parameters used, this is 34 ppm at 1550 nm). Interestingly, the backscattering from one polarization of the fundamental mode into its orthogonal polarization is less than 10 dB below the backscatter into self, indicating that in the glass regions alone, the mode fields are not mutually orthogonal.

Assuming here an arbitrary cut-off frequency of $\kappa_c = 1/(0.5\text{ mm})$ for the frozen-in surface capillary wave spectrum in Eq. 14 (or $\Lambda_c = \pi$ mm) and $T_g/\gamma = 1500$ K/J.m^{-2}, we plot in Fig. 5 the backscattering coefficient from surface roughness in the two fibers (note that the cut-off does not influence the results because $\Delta\beta$ is very large for back-propagating modes[36]). For both geometries considered here, the surface capillary wave roughness-induced backscattering from the HE_{11} mode to itself is −114 dB/m at 1550 nm, four orders of magnitude below the SMF, and in reasonable agreement with recently reported measurements[6]. We also note that the total backscattering into the LP_{11} mode group is approximately 7 dB higher. Here too, the backscatter into the orthogonal polarization of the fundamental mode is only 10 dB or so below the backscatter into itself. The three contributions are further discussed in greater detail in the following section.

IV. DISCUSSION

Figure 6 shows how the various contributions to backscattering scale as a function of the core size in NANFs with a membrane thickness of 400 nm at the fixed wavelength of 1550 nm. The markers are the results from finite element simulations as discussed above. Also shown on the figure, in solid lines, are the approximate scaling relations we derived in Eqs. 15, 16, and 17, which as can be seen agree very well with the numerical results.

Of the three mechanisms contributing to backscattering, volumetric backscattering from the hollow regions (here assumed to be filled with air at room temperature and atmospheric pressure) is the largest at approximately −100 dB/m for a 35 μm core diameter antiresonant fiber. However, an important difference with scattering in glass or from its interfaces is that the scatterers in a gas-filled hollow region are not static. The consequence of the thermal motion of the gas molecules is a Doppler broadening of the scattered signal ($\approx$ 500 MHz at room temperature). Such a broadening may 'blur' this signal when using, e.g., interferometric measurement schemes such as optical frequency domain reflectometry, OFDR, when it is large compared to the measurement bandwidth (the latter is determined by chirp rate, fiber length, etc). However, techniques that rely only on the amplitude measurement such as optical time domain reflectometry, OTDR should allow for straightforward measurement and analysis of this contribution provided they have adequate sensitivity and dynamic range.

The contribution from the hollow regions can be strongly reduced, for example by evacuating the fiber. To a first approximation, the Rayleigh scattering coefficient of a gas is proportional to its pressure[13]. A pressure of 10 millibars would therefore reduce the backscattering from the air-filled core to about -120 dB/m, below the value we estimate for surface scattering which thus imposes the true fundamental limit to backscattering. For a low-loss antiresonant fiber with a core diameter of $\sim$ 35 μm, the backscattering is predicted to be nearly four orders of magnitude lower than in SMFs when the surface roughness originates from frozen-in thermally excited surface capillary waves. Such low levels of backscattering require the development of bespoke tools, such as the one reported in[6], for reliably characterizing these fibers for the purpose of distributed fault-finding.

For all the processes considered, the combined sum of backscattering into higher order modes is higher than that into the fundamental mode itself by a few dBs. The contribution of such higher order modes to a measured backscattered signal is however severely attenuated, first by the higher loss suffered by the higher order mode from the scattering point to the input of the fiber, and then by the filtering effect of a splice into a single mode fiber if the measurement technique employs one.

The analysis we have presented here naturally applies to other hollow-core fiber types. For the better part of the past two decades, research efforts were focused on hollow-core photonic bandgap fibers (HC-PBGFs) which rely on the photonic bandgap effect of a periodic honeycomb lattice to confine and guide light in a hollow-core. Using a variety of techniques, the measured backscattering coefficient in a commercial 7c HC-PBGFs with a core diameter of $\approx$ 11 μm was reported to be $\approx$ −60 dB/m, more than an order of magnitude above that of the single mode fiber[37,38].

We used Eqs. 9 and 13 to calculate the corresponding contribution for examples of idealized 7c and 19c HC-PBGF and show the results in Table I. We predict that the surface rough-

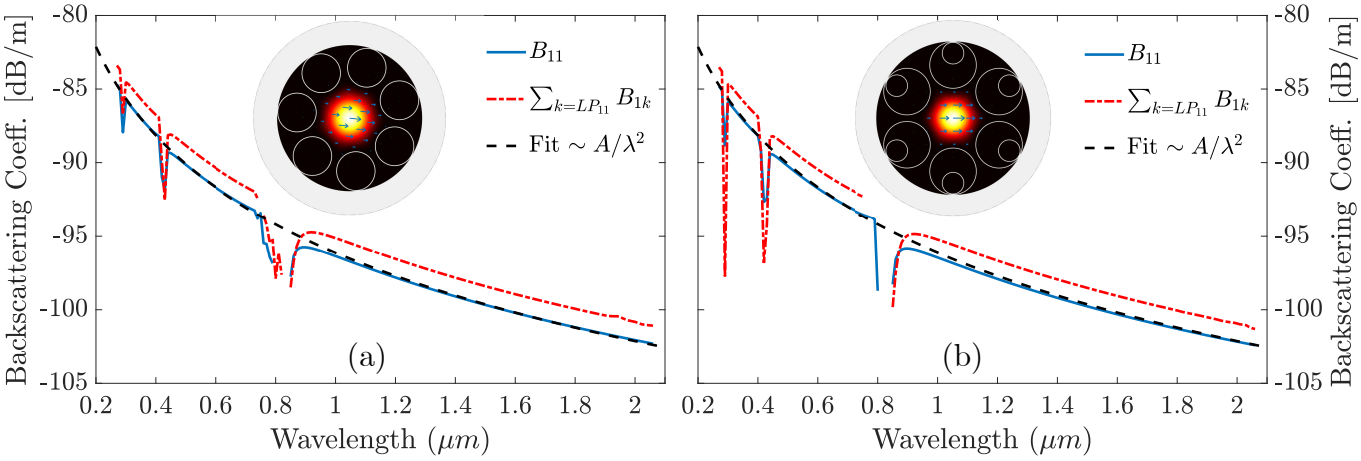

FIG. 3. Volumetric Rayleigh scattering contributions to the backscattering coefficient from the hollow regions of a tubular antiresonant fiber (a) and a NANF (b). For the calculations, we have assumed that the hollow regions are filled with air at room temperature and atmospheric pressure. For clarity, we only show the sum of the scattering into the LP_{11} mode group. The dashed black curves show the approximate scaling with wavelength derived in Eq. 15.

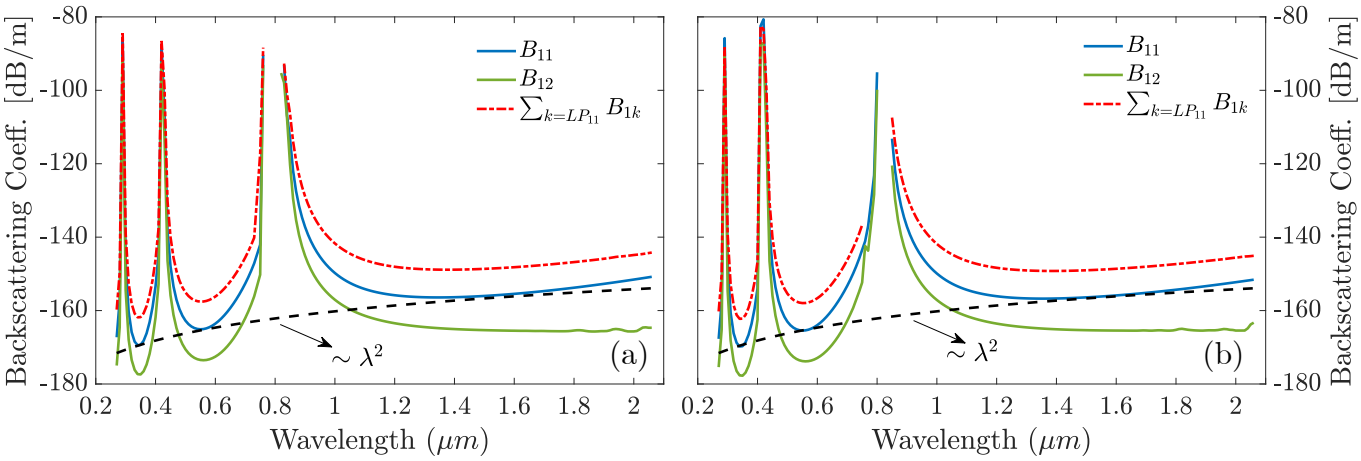

FIG. 4. Volumetric Rayleigh scattering contributions to the backscattering coefficient from the glass regions in a tubular fiber (a) and in a NANF (b). The scattering into the other polarization of the fundamental mode is shown in green. The dashed black curves show the scaling with wavelength derived in Eq. 16.

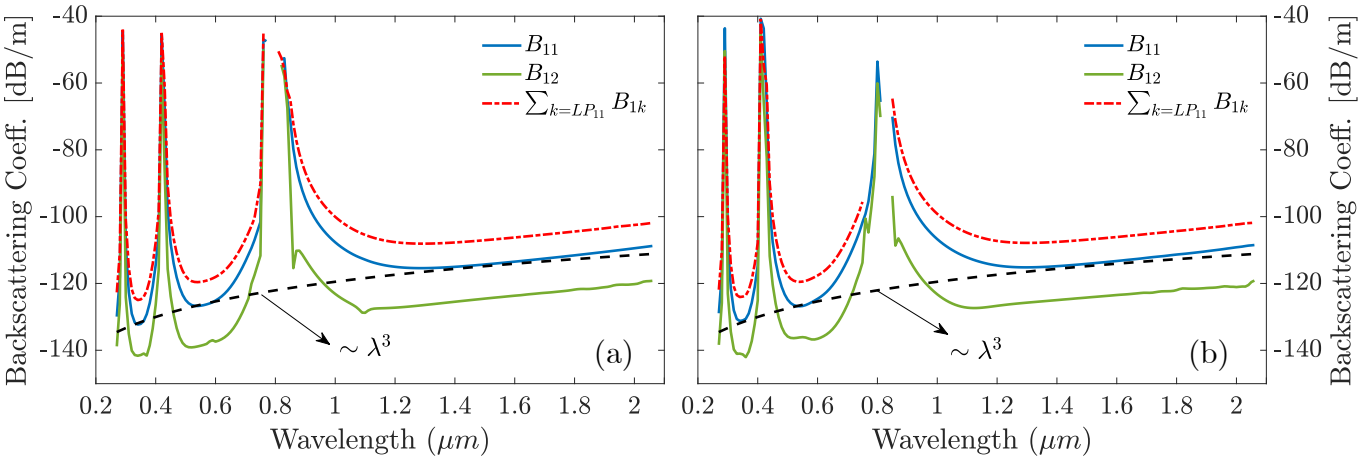

FIG. 5. Surface roughness scattering contributions to the backscattering coefficient in a tubular fiber (a) and in NANF (b). The dashed black line shows the approximate scaling with wavelength from Eq. 17.

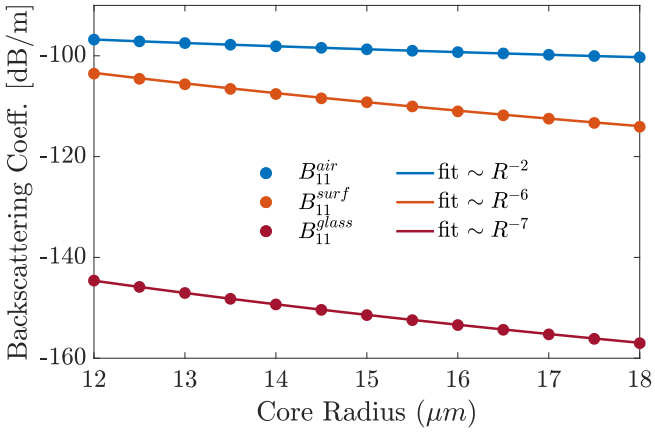

FIG. 6. Backscattering coefficient of a NANF as a function of core size. The hollow regions of the fiber are assumed to be filled with air at room temperature and atmospheric pressure. The markers show finite element calculations whilst the solid lines are scaling relations from Eqs. 15, 16, and 17.

ness dominated backscattering coefficient in a 7c fiber is similar to that of SMFs whilst that of the 19c is some 17 dB lower. These are approximately 10 dB higher than NANFs with similar core diameters and originate primarily from the stronger field intensity near the air-glass interfaces. Our predictions for the 7c HC-PBGFs which use the power spectrum of Eq. 14 are lower than have been reported by more than 15 dB. This difference has been speculatively ascribed to potential core diameter fluctuations with a few centimeter correlation length or significantly higher roughness power spectrum in HC-PBGFs[39,40]. We note however, that very small changes in the HC-PBGF structure, especially in its core surround can introduce surface modes and cause a dramatic increase in the field intensity near the air-glass interfaces, leading to higher loss and backscattering than in symmetric and regular structures. That this problem is removed entirely in nodeless antiresonant fibers is the reason why their experimentally measured properties can more closely approach the fundamental limits, both in terms of loss, backscattering, nonlinearity, etc.

TABLE I. **Backscattering coefficient for HC-PBGFs**

Core diameter	Loss (dB/km)	B_{11}^{air}	B_{11}^{glass}	B_{11}^{surf}
7c (11.5μm)	21	-90	-105	-75
19c (20μm)	5	-94	-119	-90

V. CONCLUSION

We have presented a theoretical analysis of the fundamental mechanisms driving backscattering in hollow-core antiresonant fibers, making the distinction between volume contributions and that from surface roughness scattering. We showed through two examples that the key parameters driving backscattering in this class of fibers are the core diameter, thickness of the antiresonant membranes as well as the optical wavelength, with the exact geometry of the antiresonant cladding playing a negligible role. Scaling relations with wavelength and core diameter were shown to match extremely well the results of finite element simulations.

Our analysis has revealed that when filled with a gas, for example air at atmospheric pressure and room temperature, the backscatter from the hollow regions of the fiber provide the dominant contributions. However, because scatterers in gases are not static and given that they can be removed for example by evacuating the fiber, the true fundamental limit to backscatter in these fibers is imposed by scattering from the intrinsic roughness on the glass surfaces, with the bulk scattering from the glass regions contributing negligibly.

We estimate this fundamental contribution to backscattering to be more than four orders of magnitude lower than in the standard SMF, in good agreement with recently reported measurements. Such low predicted and measured backscattering levels in these fibers would enable a drastic reduction in backscattering induced errors in interferometric sensors such as gyroscopes and other applications where bidirectional propagation is required.

Such reduced backscattering levels require improvements in the sensitivity of reflectometry tools for routine hollow-core fiber or cable characterization. In this sense, the distinction we make between the contribution from dynamic scatterers in gas-filled hollow regions, and static ones on the surface or within the glass material is an important one. The former is more than 10 dB higher than the latter for core diameters larger than 30 µm (for air at room temperature and atmospheric pressure) and can be measured with time domain reflectometers. The latter however, requires more sensitive instruments to measure accurately.

Beyond backscattering, the theoretical analysis presented here will be useful in discussing the fundamental limitations on other propagation effects within the fiber such as the intermodal cross-talk and its impact on the performance of communication links which incorporate current and next-generation antiresonant fibers.

ACKNOWLEDGEMENTS

Funding sources: Engineering and Physical Sciences Research Council (EP/P030181/1); European Research Council (682724); Fonds de recherche du Québec – Nature et technologies; Natural Sciences and Engineering Research Council of Canada.

E. N. F. and R. S. acknowledge support from the UK Royal Academy of Engineering Research and Senior Research Fellowships. V. M. B. acknowledges support from the Vanier Canada Graduate Scholarship program.

The data that support the findings of this study are openly available in the University of Southampton's repository at http://doi.org/xxxxxx.

[1]G. T. Jasion, T. D. Bradley, K. Harrington, H. Sakr, Y. Chen, E. Numkam Fokoua, I. A. Davidson, A. Taranta, J. R. Hayes, D. J. Richardson, and F. Poletti, "Hollow core nanf with 0.28 db/km attenuation in the

c and l bands," in *Optical Fiber Communication Conference Postdeadline Papers 2020* (Optical Society of America, 2020) p. Th4B.4.

[2]H. Sakr, Y. Chen, G. T. Jasion, T. D. Bradley, J. R. Hayes, H. C. H. Mulvad, I. A. Davidson, E. Numkam Fokoua, and F. Poletti, "Hollow core optical fibres with comparable attenuation to silica fibres between 600 and 1100nm," Nature Communications **11** (2020), 10.1038/s41467-020-19910-7.

[3]S.-f. Gao, Y.-y. Wang, W. Ding, Y.-f. Hong, and P. Wang, "Conquering the Rayleigh Scattering Limit of Silica Glass Fiber at Visible Wavelengths with a Hollow-Core Fiber Approach," Laser and Photonics Reviews **14** (2020), 10.1002/lpor.201900241.

[4]H. Sakr, T. D. Bradley, G. T. Jasion, E. N. Fokoua, S. R. Sandoghchi, I. A. Davidson, A. Taranta, G. Guerra, W. Shere, Y. Chen, J. R. Hayes, D. J. Richardson, and F. Poletti, "Hollow core nanfs with five nested tubes and record low loss at 850, 1060, 1300 and 1625nm," in *2021 Optical Fiber Communications Conference and Exhibition (OFC)* (2021) pp. 1–3.

[5]A. Taranta, E. Numkam Fokoua, S. A. Mousavi, J. R. Hayes, T. D. Bradley, G. T. Jasion, and F. Poletti, "Exceptional polarization purity in antiresonant hollow-core optical fibres," Nature Photonics **14**, 504+ (2020).

[6]V. Michaud-Belleau, E. Numkam Fokoua, T. D. Bradley, J. R. Hayes, Y. Chen, F. Poletti, D. J. Richardson, J. Genest, and R. Slavík, "Backscattering in antiresonant hollow-core fibers: over 40 dB lower than in standard optical fibers," Optica **8**, 216 (2021).

[7]G. A. Sanders, A. A. Taranta, C. Narayanan, E. Numkam Fokoua, S. A. Mousavi, L. K. Strandjord, M. Smiciklas, T. D. Bradley, J. Hayes, G. T. Jasion, T. Qiu, W. Williams, F. Poletti, and D. N. Payne, "Hollow-core resonator fiber optic gyroscope using nodeless anti-resonant fiber," Optics Letters **46**, 46–49 (2021).

[8]J. H. Chow, I. C. M. Littler, D. E. McClelland, and M. B. Gray, "Laser frequency-noise-limited ultrahigh resolution remote fiber sensing," Opt. Express **14**, 4617–4624 (2006).

[9]Ł. Śliwczyński, P. Krehlik, and M. Lipiński, "Optical fibers in time and frequency transfer," Measurement Science and Technology **21**, 075302 (2010).

[10]S.-f. Gao, Y. Wang, W. Ding, D.-l. Jiang, S. Gu, X. Zhang, and P. Wang, "Hollow-core conjoined-tube negative-curvature fibre with ultralow loss," Nature Communications **9**, 1–6 (2018).

[11]F. Amrani, J. H. Osório, F. Delahaye, F. Giovanardi, L. Vincetti, B. Debord, F. Gérôme, and F. Benabid, "Low-loss single-mode hybrid-lattice hollow-core photonic-crystal fibre," Light: Science and Applications **10** (2021), 10.1038/s41377-020-00457-7, 2006.06375.

[12]P. J. Roberts, F. Couny, H. Sabert, B. J. Mangan, D. P. Williams, L. Farr, M. W. Mason, A. Tomlinson, T. A. Birks, J. C. Knight, and P. S. J. Russell, "Ultimate low loss of hollow-core photonic crystal fibres," Optics Express **13**, 236–244 (2005).

[13]D. Marcuse, *Theory of Dielectric Optical Waveguides*, 2nd ed. (Academic Press, 1991).

[14]A. W. Snyder and J. D. Love, *Optical Waveguide Theory* (Chapman and Hall Ltd, 1983).

[15]A. W. Snyder, "Radiation Losses Due To Variations Of Radius On Dielectric Or Optical Fibers," IEEE Transactions On Microwave Theory And Techniques **MT18**, 608–615 (1970).

[16]I. A. White, "Radiation From Bends In Optical-waveguides - Volume-current Method," IEE Journal on Microwaves Optics and Acoustics **3**, 186–188 (1979).

[17]M. Kuznetsov and H. A. Haus, "Radiation Loss In Dielectric Waveguide Structures By The Volume Current Method," IEEE Journal of Quantum Electronics **19**, 1505–1514 (1983).

[18]J. P. R. Lacey and F. P. Payne, "Radiation loss from planar waveguides with random wall imperfections," IEE Proceedings **137**, 282–288 (1990).

[19]P. R. McIsaac, "Mode Orthogonality in Reciprocal and Nonreciprocal Waveguides," IEEE Transactions on Microwave Theory and Techniques **39**, 1808–1816 (1991).

[20]S. G. Johnson, M. Ibanescu, M. Skorobogatiy, O. Weisberg, T. D. Engeness, M. Soljacic, S. A. Jacobs, J. D. Joannopoulos, and Y. Fink, "Low-loss asymptotically single-mode propagation in large-core omniguide fibers," Optics Express **9**, 748–779 (2001).

[21]M. Nakazawa, "Rayleigh Backscattering Theory for Single-Mode Optical Fibers." Journal of the Optical Society of America **73**, 1175–1180 (1983).

[22]M. R. Henderson, S. Afshar V., A. D. Greentree, and T. M. Monro, "Dipole emitters in fiber: interface effects, collection efficiency and optimization," Optics Express **19**, 16182 (2011).

[23]S. G. Johnson, M. L. Povinelli, M. Soljačić, A. Karalis, S. Jacobs, and J. D. Joannopoulos, "Roughness losses and volume-current methods in photonic-crystal waveguides," Applied Physics B: Lasers and Optics **81**, 283–293 (2005).

[24]D. Marcuse, "Rayleigh Scattering and the Impulse Response of Optical Fibers," Bell System Technical Journal **53**, 705–715 (1974).

[25]Z. Wang, H. Wu, X. Hu, N. Zhao, Q. Mo, and G. Li, "Rayleigh scattering in few-mode optical fibers," Scientific Reports **6**, 1–8 (2016).

[26]E. Brinkmeyer, "Analysis of the backscattering method for single-mode optical fibers," J. Opt. Soc. Am. **70**, 1010–1012 (1980).

[27]A. Hartog and M. Gold, "On the theory of backscattering in single-mode optical fibers," Journal of Lightwave Technology **2**, 76–82 (1984).

[28]J. Jäckle and K. Kawasaki, "Intrinsic roughness of glass surfaces," Journal of Physics - condensed Matter **7**, 4351–4358 (1995).

[29]S. G. Johnson, M. Ibanescu, M. A. Skorobogatiy, O. Weisberg, J. D. Joannopoulos, and Y. Fink, "Perturbation theory for Maxwell's equations with shifting material boundaries," Physical Review E - Statistical Physics, Plasmas, Fluids, and Related Interdisciplinary Topics **65**, 1–7 (2002).

[30]P. J. Roberts, F. Couny, H. Sabert, B. J. Mangan, T. A. Birks, J. C. Knight, and P. S. Russell, "Loss in solid-core photonic crystal fibers due to interface roughness scattering," Optics Express **13**, 7779–7793 (2005).

[31]E. A. J. Marcatili and R. A. Schmeltzer, "Hollow metallic and dielectric waveguides for long distance optical transmission and lasers," Bell System Technical Journal **43**, 1783–1809 (1964).

[32]`https://www.corning.com/media/worldwide/coc/documents/Fiber/PI-1463-AEN.pdf`.

[33]M. Ohashi, K. Shiraki, and K. Tajima, "Optical loss property of silica-based single-mode fibers," Journal of Lightwave Technology **10**, 539–543 (1992).

[34]F. Poletti, "Nested antiresonant nodeless hollow core fiber," Opt. Express **22**, 23807–23828 (2014).

[35]A. Bucholtz, "Rayleigh-scattering calculations for the terrestrial atmosphere," Applied Optics **34**, 2765 (1995).

[36]E. N. Fokoua, F. Poletti, and D. J. Richardson, "Analysis of light scattering from surface roughness in hollow-core photonic bandgap fibers," Opt. Express **20**, 20980–20991 (2012).

[37]S. W. Lloyd, V. Dangui, M. J. F. Digonnet, S. Fan, and G. S. Kino, "Measurement of reduced backscattering noise in laser-driven fiber optic gyroscopes," Optics Letters **35**, 121 (2010).

[38]X. Xu, M. Yan, N. Song, C. Wu, F. Teng, and J. Jin, "Measurement of Backscattering in Hollow Core Photonic Bandgap Fiber Based on Mach-Zehnder and Michelson Hybrid Interferometer," IEEE Photonics Technology Letters **28**, 2858–2861 (2016).

[39]V. Dangui, M. J. Digonnet, and G. S. Kino, "Modeling of the propagation loss and backscattering in air-core photonic-bandgap fibers," Journal of Lightwave Technology **27**, 3783–3789 (2009).

[40]K. Zamani Aghaie, M. J. F. Digonnet, and S. Fan, "Modeling loss and backscattering in a photonic-bandgap fiber using strong perturbation," Photonic and Phononic Properties of Engineered Nanostructures III **8632**, 86320K (2013).